Mechanical Systems and Signal Processing 43 (2014) 237–245

Contents lists available at ScienceDirect

Mechanical Systems and Signal Processing

journal homepage: www.elsevier.com/locate/ymssp

On the use of the H_s estimator for the experimental assessment of transmissibility matrices

Q. Leclère [a,*], N.B. Roozen [b,c], C. Sandier [a]

[a] Laboratoire Vibrations Acoustique, INSA-Lyon, 25 bis Avenue Jean Capelle, F-69621 Villeurbanne, Cedex, France
[b] Katholieke Universiteit Leuven, Department of Mechanical Engineering, Box 2420, Celestijnenlaan 300 B, B-3001 Leuven, Belgium
[c] Delft University of Technology, Faculty of Aerospace Engineering, Kluyverweg 1, 2629 HS Delft, The Netherlands

ARTICLE INFO

Article history:
Received 8 July 2012
Accepted 19 September 2013
Available online 11 October 2013

Keywords:
Transmissibility matrix
MIMO systems
H_s estimator

ABSTRACT

The experimental estimation of frequency response functions characterizing SISO linear systems is a well established topic. Several estimators are defined in the literature, each estimator being optimal depending upon the assumptions with respect to the balance of noise between the input and output of the system. H_1 and H_2 have to be used in case of presence of noise on output and input, respectively. The H_V or H_s estimator is chosen if input and output are assumed to have equivalent SNR. These estimators are also established for MIMO linear systems, with additional difficulties due to the necessity of inversing cross spectral matrices. A transmissibility function is generally defined as a linear relationship between two outputs of a linear system. For MIMO systems, transmissibilities are not defined by the system only, it also depends on the input quantities. It is however possible to define a transmissibility matrix between two sets of outputs that is, under some assumptions, uniquely defined. This approach is especially the base of Operational Transfer Path analysis, an engineering method benefiting of a strong research effort in the last few years. This paper deals with the use of the application of MIMO system estimators to the experimental assessment of transmissibility matrices. Transmissibility matrices are generally estimated using a H_1 like approach in the literature. The possibility of using H_2 and H_s is presented in this work, from the theoretical point of view and with numerical and practical illustrations.

1. Introduction

The transmissibility functions are generally defined as linear relationships between two responses of a linear system. They have particular properties, in comparison with standard transfer functions representing classical excitation–response relationships. The standard transfer function, for instance, is entirely defined by the studied system, while transmissibility between two responses depends also on the excitation configuration. Another important difference is that the standard transfer functions have peaks at the resonances of the system, while transmissibilities have peaks at frequencies corresponding to zeros of one of the considered response. Transmissibilities are thus more difficult to handle, but they are also easier to measure, because it is generally easier to mount a response sensor than an excitation sensor (which has to be inserted between the excitation device and the structure). That's why several transmissibility based methods have been developed in the literature, for instance in structural health monitoring [1], output only modal analysis [2,3], or Operational

* Corresponding author. Tel.: +33 47 24 36 392; fax: +33 4 72 43 87 12.
E-mail address: quentin.leclere@insa-lyon.fr (Q. Leclère).

0888-3270/$ - see front matter © 2013 Elsevier Ltd. All rights reserved.
http://dx.doi.org/10.1016/j.ymssp.2013.09.008

Transfer Path Analysis [4,5], in which the concept of transmissibility functions has to be extended to transmissibility matrices [6] between two sets of responses. The present work focusses on the experimental estimation of such transmissibility matrices.

Several estimators are known for the experimental assessment of transfer functions between one input and one output: H_1 has to be used when the noise is on the output and H_2 when the noise is on the input [7]. Another estimator, H_s, has been proposed by Wicks and Vold [8], based on a total least squares approach, that consider noise on both the input and the output. This estimator has been extended to MIMO systems in [9,10]. The H_s approach seems particularly interesting for the estimation of transmissibility matrices, because the inputs and outputs of a transmissibility system are both responses, the SNR (Signal to Noise Ratio) has thus no reason to be higher on input or output responses.

The general principles of the transmissibility matrix approach is briefly treated in the first section of the paper. Then the concept of H_1, H_2, and H_s estimates for transmissibility matrices is addressed from a theoretical point of view. The two last parts are dedicated to numerical and experimental illustrations, respectively.

N.B.: Throughout this paper, bold capitals are used for matrices (including vectors) and non-bold capitals for scalars. Note that all matrices are dependent upon frequency. For sake of brevity this dependency is not mentioned explicitly in the equations.

2. Transmissibility matrices: definition

Let us consider a linear dynamic system relating a set of n excitation dofs $\mathbf{F}$ (size $n \times 1$) to two different sets of response dofs, named indicator dofs $\mathbf{Y}$ ($n \times 1$) and output dofs $\mathbf{X}$ ($m \times 1$):

$$\begin{bmatrix}\mathbf{X}\\ \mathbf{Y}\end{bmatrix} = \begin{bmatrix}\mathbf{H}\\ \mathbf{\Phi}\end{bmatrix}\mathbf{F} \tag{1}$$

where $\mathbf{\Phi}$ and $\mathbf{H}$ are transfer matrices relating excitation dofs to response dofs. A linear relationship can be then defined between $\mathbf{X}$ and $\mathbf{Y}$, under the condition of invertibility of $\mathbf{\Phi}$:

$$\mathbf{X} = \mathbf{H}\mathbf{\Phi}^{-1}\mathbf{Y} = \mathbf{T}\mathbf{Y} \tag{2}$$

where $\mathbf{T} = \mathbf{H}\mathbf{\Phi}^{-1}$ is the transmissibility matrix and where $^{-1}$ denotes a matrix inverse. The existence of $\mathbf{T}$ thus depends on these two major conditions:

- the definition of a set of excitation dofs $\mathbf{F}$
- the invertibility of matrix $\mathbf{\Phi}$ relating $\mathbf{Y}$ to $\mathbf{F}$

3. Transmissibility matrices: experimental estimation

3.1. Methodology

The relation (2) between inputs and outputs can be written using cross spectral matrices

$$\mathbf{G_{xy}} = \mathbf{T}\mathbf{G_{yy}} \tag{3}$$

$$\mathbf{G_{xx}} = \mathbf{T}\mathbf{G_{yx}} \tag{4}$$

where element (p,q) of matrix $\mathbf{G_{xy}}$ is the cross spectrum between the pth element of $\mathbf{X}$ and the qth element of $\mathbf{Y}$. However, the cross-spectral matrices obtained for a single operational condition are in general non invertible. Matrices $\mathbf{G_{yy}}$ and $\mathbf{G_{yx}}$ are indeed rarely of full rank and even less often well conditioned. A potential solution to this problem is to assess transmissibility matrices from non-stationary operating conditions, like run-up or down.

One approach is to gather several steady-state operating condition in one system:

$$\mathbf{X_K} = [\mathbf{X}_1\mathbf{X}_2\ldots\mathbf{X}_k] \quad \mathbf{Y_K} = [\mathbf{Y}_1\mathbf{Y}_2\ldots\mathbf{Y}_k]$$

where $\mathbf{X}_i$ and $\mathbf{Y}_i$ are response vectors obtained during one operating condition, using a phase reference sensor or more sophisticated techniques like Conditioned Spectral Analysis [7] or Virtual Source Analysis [11]. If more than one uncorrelated processes are identified (this is the case if the coherence function between channels is not close to unity), several response vectors can be extracted from each acquisition. Finally, cross spectral matrices can still be calculated from such results:

$$\mathbf{G_{xy}} = \mathbf{X_K}\mathbf{Y_K}' \quad \mathbf{G_{yy}} = \mathbf{Y_K}\mathbf{Y_K}' \quad \mathbf{G}_{xx} = \mathbf{X_K}\mathbf{X_K}T'$$

where $'$ denotes the complex conjugate transpose. The experimental assessment of these matrices is not always easy, because the computation of T requires inversions of these matrices, that have to be consequently of full rank. This condition is rarely fulfilled using only one operating condition of the studied system; as was said earlier, it is often necessary to gather information from several operating conditions, using several steady state operating points or run-up-down acquisitions.

3.2. H_1 and H_2 estimators

For a scalar transfer function, the H_1 and H_2 estimators are given by

$$H_1[T] = G_{xy}G_{yy}^{-1} \tag{5}$$

$$H_2[T] = G_{xx}G_{yx}^{-1} \tag{6}$$

The H_1 and H_2 estimates of the transmissibility matrix are, by analogy to Eqs. (5) and (6) and by inversion of systems (3) and (4), defined by

$$H_1[\mathbf{T}] = \mathbf{G_{xy}}\mathbf{G_{yy}}^{-1} \tag{7}$$

$$H_2[\mathbf{T}] = \mathbf{G}_{xx}\ \mathbf{G}_{yx}^{+} = \mathbf{G}_{xx}\ \mathbf{G}_{yx}(\mathbf{G}_{yx}\ \mathbf{G_{xy}})^{-1} \tag{8}$$

where $^+$ denotes the pseudo-inverse. It is worth noting that the estimator $H_2[\mathbf{T}]$ requires $m \geq n$, which is a necessary condition for $(\mathbf{G}_{yx}\ \mathbf{G_{xy}})$ to be of full rank.

3.3. H_s estimator

For a scalar transfer function, the H_s estimator is based on the eigenvalue decomposition of

$$\begin{bmatrix} s^2G_{xx} & sG_{xy} \\ sG_{yx} & G_{yy} \end{bmatrix} = \begin{bmatrix} U_x & V_x \\ U_y & V_y \end{bmatrix} \begin{bmatrix} \lambda_1 & 0 \\ 0 & \lambda_2 \end{bmatrix} \begin{bmatrix} U_x & V_x \\ U_y & V_y \end{bmatrix}'$$

where s is a positive scaling factor used to balance the magnitude of x and y. Assuming that the smallest eigenvalue is representing noise, H_s is defined as the ratio between contributions of the largest eigenvalue (λ_1) at x and y:

$$H_s = \frac{U_x}{sU_y} \tag{9}$$

which is explicitly given by the both following formulas:

$$H_s = \frac{s^2G_{xx} - G_{yy} + \sqrt{(s^2G_{xx} - G_{yy})^2 + 4s^2|G_{yx}|^2}}{2s^2G_{yx}} \tag{10}$$

$$= \frac{2G_{xy}}{G_{yy} - s^2G_{xx} + \sqrt{(s^2G_{xx} - G_{yy})^2 + 4s^2|G_{yx}|^2}} \tag{11}$$

It can be noted that Eq. (10) is equivalent to H_2 when $s \to \infty$, and that Eq. (11) is equal to H_1 when $s = 0$.

The H_s estimate of the transmissibility matrix is based on an analysis of the physical rank of the global cross spectral matrix. The system (1) can be formulated in terms of cross spectra:

$$\mathbf{G_{xyxy}} = \begin{bmatrix} \mathbf{G}_{xx} & \mathbf{G_{xy}} \\ \mathbf{G}_{yx} & \mathbf{G_{yy}} \end{bmatrix} = \begin{bmatrix} \mathbf{H} \\ \Phi \end{bmatrix} \mathbf{S_{ff}} \begin{bmatrix} \mathbf{H} \\ \Phi \end{bmatrix}' \tag{12}$$

The columns of $\mathbf{G_{xyxy}}$ are thus linear combinations of the columns of $[\mathbf{H}'\Phi']'$. The rank of $\mathbf{G_{xyxy}}$ cannot be greater than the number of input loads. The H_s estimate of the transmissibility matrix is obtained from the following scaled eigenvalue decomposition:

$$\begin{bmatrix} \mathbf{s_x} & 0 \\ 0 & \mathbf{s_y} \end{bmatrix} \begin{bmatrix} \mathbf{G_{xx}} & \mathbf{G_{xy}} \\ \mathbf{G_{yx}} & \mathbf{G_{yy}} \end{bmatrix} \begin{bmatrix} \mathbf{s_x} & 0 \\ 0 & \mathbf{s_y} \end{bmatrix} = \begin{bmatrix} \mathbf{U} \\ \mathbf{V} \end{bmatrix} \mathbf{\Lambda} \begin{bmatrix} \mathbf{U} \\ \mathbf{V} \end{bmatrix}' \tag{13}$$

where $\mathbf{\Lambda}$ is the diagonal matrix of eigenvalues, $[\mathbf{U}'\mathbf{V}']'$ the matrix of eigenvectors, and $\mathbf{s_x}$ and $\mathbf{s_y}$ diagonal scaling matrices. Considering that the number of input loads is equal to n (as well as the number of indicators $\mathbf{Y}$), the rank of the (scaled) $\mathbf{G_{xyxy}}$ matrix is lower or equal to n. The m smallest singular values of $\mathbf{\Lambda}$ are thus considered as representing noise, and can be rejected:

$$\begin{bmatrix} \mathbf{U_n} \\ \mathbf{V_n} \end{bmatrix} \mathbf{\Lambda}_n \begin{bmatrix} \mathbf{U_n} \\ \mathbf{V_n} \end{bmatrix}' = \begin{bmatrix} \mathbf{s_x} & 0 \\ 0 & \mathbf{s_y} \end{bmatrix} \begin{bmatrix} \mathbf{H} \\ \Phi \end{bmatrix} \mathbf{S_{ff}} \begin{bmatrix} \mathbf{H} \\ \Phi \end{bmatrix}' \begin{bmatrix} \mathbf{s_x} & 0 \\ 0 & \mathbf{s_y} \end{bmatrix}, \tag{14}$$

where $\mathbf{\Lambda}_n$ the diagonal matrix of the n largest eigenvalues and $[\mathbf{U_n}'\mathbf{V_n}']'$ are the n corresponding eigenvectors. Let us write for convenience the eigenvalue decomposition of the cross spectral matrix of unknown forces:

$$\mathbf{S_{ff}} = \mathbf{P\Sigma P}'$$

System (14) can be written as follows:

$$\begin{cases} \mathbf{U_n}\boldsymbol{\Lambda_n}\mathbf{U_n'} = \mathbf{s_x}\mathbf{H}\boldsymbol{\Psi}\boldsymbol{\Sigma}\mathbf{P}'\mathbf{H}'\mathbf{s_x} \\ \mathbf{V_n}\boldsymbol{\Lambda_n}\mathbf{V_n'} = \mathbf{s_y}\boldsymbol{\Phi}\mathbf{P}\boldsymbol{\Sigma}\mathbf{P}'\boldsymbol{\Phi}'\mathbf{s_y} \end{cases} \tag{15}$$

that can be written in a more simple way

$$\begin{cases} \mathbf{U_n}\boldsymbol{\Lambda_n}^{1/2} = \mathbf{s_x}\mathbf{H}\mathbf{P}\boldsymbol{\Sigma}^{1/2} \\ \mathbf{V_n}\boldsymbol{\Lambda_n}^{1/2} = \mathbf{s_y}\boldsymbol{\Phi}\mathbf{P}\boldsymbol{\Sigma}^{1/2} \end{cases} \tag{16}$$

Then, $\boldsymbol{\Phi}^{-1}$ and $\mathbf{H}$ are expressed as follows:

$$\begin{cases} \mathbf{H} = \mathbf{s_x}^{-1}\mathbf{U_n}\boldsymbol{\Lambda_n}^{1/2}\boldsymbol{\Sigma}^{-1/2}\mathbf{P}' \\ \boldsymbol{\Phi}^{-1} = \mathbf{P}\boldsymbol{\Sigma}^{1/2}\boldsymbol{\Lambda_n}^{-1/2}\mathbf{V_n}^{-1}\mathbf{s_y} \end{cases} \tag{17}$$

to finally obtain the expression of $H_s[\mathbf{T}]$

$$H_s[\mathbf{T}] = \mathbf{H}\boldsymbol{\Phi}^{-1} = \mathbf{s_x}^{-1}\mathbf{U_n}\mathbf{V_n}^{-1}\mathbf{s_y} \tag{18}$$

It can be noted that if response vectors are extracted from several operating conditions to build $\mathbf{X_K}$ and $\mathbf{Y_K}$, the eigenvector decomposition of the whole matrix given by Eq. (13) can be replaced by the singular value decomposition:

$$\begin{bmatrix} \mathbf{s_x}\mathbf{X_K} \\ \mathbf{s_y}\mathbf{Y_K} \end{bmatrix} = \begin{bmatrix} \mathbf{U} \\ \mathbf{V} \end{bmatrix} \mathbf{A}\mathbf{W}' = \begin{bmatrix} \mathbf{U} \\ \mathbf{V} \end{bmatrix} \boldsymbol{\Psi}, \tag{19}$$

where $[\mathbf{U}'\mathbf{V}']\left[\begin{smallmatrix}\mathbf{U}\\\mathbf{V}\end{smallmatrix}\right] = \mathbf{I}$, $\mathbf{W}\mathbf{W}' = \mathbf{I}$, and $\mathbf{A}$ is the diagonal matrix of singular values. The product $\mathbf{A}\mathbf{W}' = \boldsymbol{\Psi}$ can be considered as a matrix of forces, and $\mathbf{U}$ and $\mathbf{V}$ as transfer matrices between $\boldsymbol{\Psi}$ and responses, respectively $\mathbf{X_K}$ and $\mathbf{Y_K}$ (cf. Eq. (1)). Considering the number of forces exciting the structure equal to n as an a priori information, the m smallest singular values can be zeroed. Finally, noting $[\mathbf{U_n'}\mathbf{V_n'}]'$ the left singular vectors corresponding to the n largest singular values, the expression of $H_s[\mathbf{T}]$ is the same as in Eq. (18). The computation of $\mathbf{U_n}$ and $\mathbf{V_n}$ leads indeed to equal results based on the eigen-decomposition of the whole cross spectral matrix (Eq. (13)) or from the singular value decomposition of the response vectors (Eq. (19)).

3.4. Effects of scaling matrices on H_s

The truncation of singular values can be seen as a way to denoise measurements, because smallest zeroed ones are considered as representing noise. The denoised $\mathbf{X_K}$ and $\mathbf{Y_K}$ matrices, noted $\tilde{\mathbf{Y}}_\mathbf{K}$ and $\tilde{\mathbf{Y}}_\mathbf{K}$, are then given by

$$\begin{bmatrix} \tilde{\mathbf{X}}_\mathbf{K} \\ \tilde{\mathbf{Y}}_\mathbf{K} \end{bmatrix} = \begin{bmatrix} \mathbf{s_x}^{-1}\mathbf{U_n} \\ \mathbf{s_y}^{-1}\mathbf{V_n} \end{bmatrix} \mathbf{A_n}\ \mathbf{W_n'} \tag{20}$$

with $\mathbf{A_n}$ the diagonal matrix of the n largest singular values, and $[\mathbf{U_n'}\mathbf{V_n'}]'$ and $\mathbf{W_n}$ the corresponding left and right singular vectors, respectively.

Let us consider scaling matrices $\mathbf{s_y} = s_y\mathbf{I}$ and $\mathbf{s_x} = s_x\mathbf{I}$, with $\varepsilon = s_x/s_y$ and $m = n$ (as many response as indicator sensors) for the sake of simplicity. Then it can be shown that

$$\lim_{\varepsilon\to 0}\mathbf{A_n} = \mathbf{A_Y} \quad \lim_{\varepsilon\to 0}\mathbf{W_n} = \mathbf{W_Y} \quad \lim_{\varepsilon\to 0}\mathbf{V_n} = s_y\mathbf{V_Y}$$
$$\lim_{\varepsilon\to \infty}\mathbf{A_n} = \mathbf{A_X} \quad \lim_{\varepsilon\to \infty}\mathbf{W_n} = \mathbf{W_X} \quad \lim_{\varepsilon\to \infty}\mathbf{U_n} = s_x\mathbf{U_X}$$

where $\mathbf{A_Y}$ and $\mathbf{W_Y}$ are singular values and right singular vectors of $\mathbf{Y_K}$, and $\mathbf{A_X}$ and $\mathbf{W_X}$ are singular values and right singular vectors of $\mathbf{X_K}$, according to following SVDs:

$$\mathbf{X_K} = \mathbf{U_X}\mathbf{A_X}\mathbf{W_X'} \quad \mathbf{Y_K} = \mathbf{V_Y}\mathbf{A_Y}\mathbf{W_Y'}$$

It means that the n largest singular values are governed by only $\mathbf{Y_K}$ when $\varepsilon\to 0$ and by only $\mathbf{X_K}$ when $\varepsilon\to\infty$. In the first case, $\tilde{\mathbf{Y}}_\mathbf{K}$ is equal to $\mathbf{Y_K}$ and rows of $\tilde{\mathbf{X}}_\mathbf{K}$ are projected on left singular vectors $\mathbf{W_Y}$. In the second case, $\tilde{\mathbf{X}}_\mathbf{K}$ is equal to $\mathbf{X_K}$ and lines of $\tilde{\mathbf{Y}}_\mathbf{K}$ are projected on left singular vectors $\mathbf{W_X}$:

$$\lim_{\varepsilon\to 0}\begin{bmatrix} \tilde{\mathbf{X}}_\mathbf{K} \\ \tilde{\mathbf{Y}}_\mathbf{K} \end{bmatrix} = \begin{bmatrix} \mathbf{X_K}\mathbf{W_Y}\mathbf{W_Y'} \\ \mathbf{Y_K} \end{bmatrix} \quad \lim_{\varepsilon\to \infty}\begin{bmatrix} \tilde{\mathbf{X}}_\mathbf{K} \\ \tilde{\mathbf{Y}}_\mathbf{K} \end{bmatrix} = \begin{bmatrix} \mathbf{X_K} \\ \mathbf{Y_K}\mathbf{W_X}\mathbf{W_X'} \end{bmatrix}$$

which means that in the former case the noise is considered as contaminating $\mathbf{X_K}$ only, and in the latter case $\mathbf{Y_K}$ only. Limits of $\mathbf{U_n}$ and $\mathbf{V_n}$ when $\varepsilon\to 0$ or ∞ are identified from the previous equations:

$$\lim_{\varepsilon\to 0}\mathbf{U_n} = s_x\mathbf{X_K}\mathbf{W_Y}\mathbf{A_Y}^{-1} \quad \lim_{\varepsilon\to \infty}\mathbf{V_n} = s_y\mathbf{Y_K}\mathbf{W_X}\mathbf{A_X}^{-1}$$

Finally, the limits of $H_s[\mathbf{T}] = \mathbf{s_x}^{-1}\mathbf{U_n}\mathbf{V_n}^{-1}\mathbf{s_y}$ when $\varepsilon \to 0$ or ∞ are obtained:

$$\lim_{\varepsilon \to 0} H_s[\mathbf{T}] = \mathbf{X_K}\mathbf{W_Y}\mathbf{A_Y}^{-1}\mathbf{V_Y'} = \mathbf{X_K}\mathbf{Y_K}^{+} = H_1[\mathbf{T}] \tag{21}$$

$$\lim_{\varepsilon \to \infty} H_s[\mathbf{T}] = \mathbf{U_X}\mathbf{A_X}(\mathbf{Y_K}\mathbf{W_X})^{-1} = \mathbf{X_K}\mathbf{X_K'}(\mathbf{Y_K}\mathbf{X_K'})^{-1} = H_2[\mathbf{T}] \tag{22}$$

These results show that the H_s estimator for transmissibility matrices has a similar behavior with respect to H_1 and H_2 than for scalar transmissibilities. When the weight $\mathbf{s_y}$ of indicator sensors increases, H_s gets similar to H_1, and when the weight $\mathbf{s_x}$ of response sensors increases, H_s gets similar to H_2. In the former case the SNR will be a priori considered to be higher on indicator sensors $\mathbf{Y_K}$ (i.e. more noise on $\mathbf{X_K}$) and in the latter case on $\mathbf{X_K}$ (i.e. more noise on $\mathbf{Y_K}$).

The correct scaling of the system has to be done with respect to noise, but also with respect to different units or overall levels of each sensor. This is crucial if different type of sensors are used, for instance accelerometers and microphones. In such a case, a global scaling has to be applied so that overall scaled levels are almost equal (see [12,13] for details). If this step is not correctly carried out, then the H_s estimator will be arbitrarily closer to H_1 or H_2, not because of SNR balance assumptions but because of strong level differences due to the use of different units.

3.5. An indicator for the validity of H_s

The validity of Eq. (14) depends on the hypothesis that the n largest eigenvalues are representing the signal, and the m smallest ones the noise. This hypothesis can be verified by inspecting the ratio between the nth eigenvalue, representing the energy of the smallest incoherent process being part of signal, and the $(n+1)$th eigenvalue representing the energy of largest noise component.

$$R = \frac{\lambda_n}{\lambda_{n+1}} = \frac{a_n^2}{a_{n+1}^2} \tag{23}$$

where λ_k is the kth largest eigenvalue of $\mathbf{\Lambda}$ in Eq. (13) and a_k is the kth largest singular value of $\mathbf{A}$ in Eq. (19). Note that this check could also be performed to verify the rank of the cross-spectral matrix in case an H_1 or an H_2 matrix estimate is used. Indeed, whilst for H_1 and H_2 only n singular values are extracted from G_{yy} and G_{yx}, respectively, it is also for these estimators of prime importance that the physical rank of the cross-spectral matrix is equal to n.

4. Numerical simulation

A numerical simulation has been conducted to validate the proposed approach. An analytic model of a thin rectangular plate ($(L_1 \times L_2) = (0.6 \times 0.5)\mathrm{m}^2$) has been used for simulations, with simply supported boundary conditions (physical parameters: aluminum, thickness 5 mm, modal damping ratio 1%). Three excitation points ($[x_1, x_2] = [0.05, 0.01]$; $[0.05, 0.4]$; $[0.45, 0.25]$) and six response points (same position as excitations for indicator responses $\mathbf{Y}$ and $[x_1, x_2] = [0.3, 0.2]$; $[0.5, 0.42]$; $[0.3, 0.1]$ for output responses $\mathbf{X}$) have been considered. The response cross spectral matrix $\mathbf{G_{xyxy}}$ has been computed using Eq. (12), using transfer matrices $\mathbf{H}$ and $\mathbf{\Phi}$ obtained with the analytical model and a cross spectral matrix $\mathbf{S_{ff}}$ of uncorrelated unitary excitations. Measurement noise is added on the cross spectral matrix, using the approach described in Appendix A. Gaussian incoherent noise is added on each indicator and output responses, with rms values adjusted to get a 30 dB SNR for all responses and with periodogram parameters $N = 3000$, $M = 100$. One element of the transmissibility matrix is drawn in Fig. 1, directly computed using Eq. (2) from noise-free $\mathbf{H}$ and $\mathbf{\Phi}$ matrices, and estimated from noisy responses $\boldsymbol{G_{xyxy}}$. All response channels are accelerations, and the global SNR is the same on all responses. Scaling factors are thus chosen equal to unity for this numerical illustration. It can be seen that H_s behaves globally better than H_1

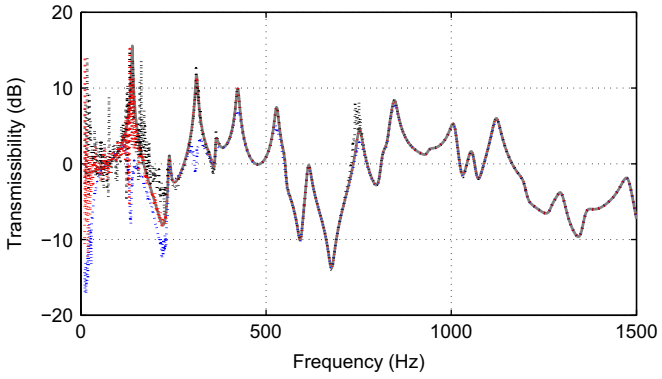

Fig. 1. #(3,1) Element of the transmissibility matrix. reference T (Solid gray) H_1 (dotted blue), H_2 (dash-dotted black) and H_s (dashed red) estimates. (For interpretation of the references to color in this figure caption, the reader is referred to the web version of this article.)

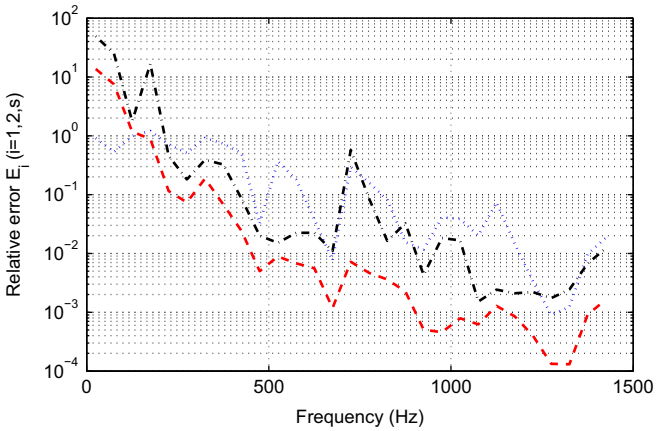

Fig. 2. 50 Hz frequency band integrated relative errors of H_1 (dotted blue), H_2 (dash-dotted black) and H_s (dashed red) estimates. (For interpretation of the references to color in this figure caption, the reader is referred to the web version of this article.)

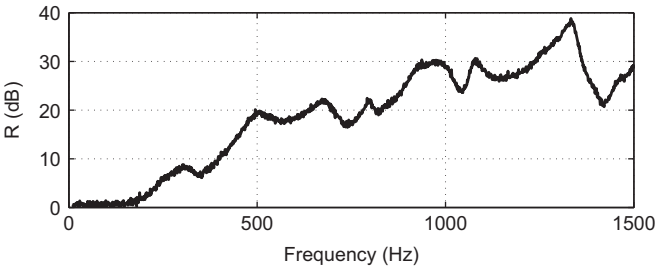

Fig. 3. H_s indicator R given by Eq. (23).

and H_2, particularly at low frequencies. In the low frequency range, the SNR is lower because the simulated response level is lower than in mid and high frequency. The global SNR is indeed fixed to 30 dB, but the noise spectral density is constant (white noise) while the simulated accelerations are more energetic in high and mid frequency than in low frequency. The SNR spectrum is thus higher in mid and high frequency than in low frequency. Above 400 Hz, the three estimations are in good agreement with the true transmissibility.

The estimation error is computed as a function of frequency for each estimator using

$$E_i(f) = \frac{\|\mathbf{T} - H_i(\mathbf{T})\|_F}{\|\mathbf{T}\|_F} \tag{24}$$

This error is drawn in Fig. 2 for $i=1,2,s$. It is clear that the error E_s is significantly lower than E_1 and E_2, except in low frequency (below 100 Hz), where E_1 is the lowest one. This can be explained by a too low SNR in low frequency. If the SNR is too low, the eigenvalues representing noise in G_{xyxy} can be higher than the eigenvalues representing the signal. In this case, keeping the n largest eigenvalues leads to an erroneous estimation of $\mathbf{T}$. This can be illustrated by the value of the H_s indicator R as introduced in Section 3.5 (see Fig. 3). This indicator R is equal to 0 dB below 200 Hz, which means that the n and $n+1$th eigenvalues are about the same level. It is thus hard to separate signal from noise. Above 200 Hz, the ratio becomes significantly greater than 1, resulting in a better estimation.

In the current case, an equal amount of noise is used on all outputs to simulate measurement noise. For this reason H_s with equal scaling factors gives the best estimate, as can be seen from Fig. 2. In case different signal-to-noise ratios are present for the indicator responses $\mathbf{Y}$ and the output responses $\mathbf{X}$, a different scaling factor for the indicator responses $\mathbf{Y}$ and the output responses $\mathbf{X}$, respectively, would in that situation give the best H_s estimate.

5. Experimental illustration

An experimental validation has been carried out to validate the proposed approach. The experiment took place in two rooms which are acoustically connected with each other by means of an aluminum plate with a thickness of 1 mm and a dimension of 60 × 40 cm. Twenty microphones – the set of output responses – were placed on the reception room side. The plate was excited from the emission room side by means of two shakers and one loudspeaker, constituting two structure borne paths and one airborne path. Two accelerometers were mounted on the plate, near shaker connection points, and one microphone was placed in the emission room: these three responses were chosen as indicators (the accelerometers for the

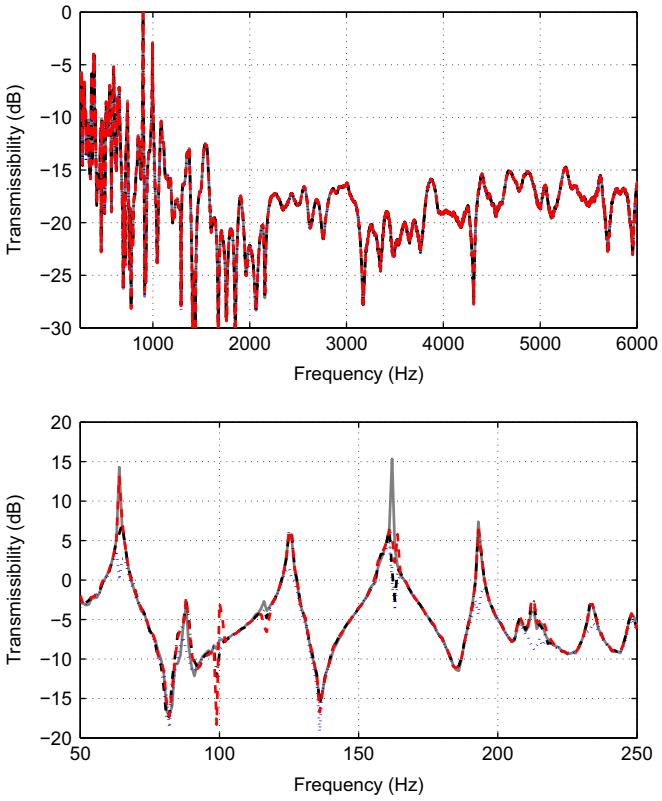

Fig. 4. #(5,2) Element of the transmissibility matrix, whole (top) and low (bottom) frequency ranges. Solid gray: T based on reference measurements, H_1 (dotted blue), H_2 (dash-dotted black) and H_s (dashed red) estimates. (For interpretation of the references to color in this figure caption, the reader is referred to the web version of this article.)

two shakers and the microphone for the loudspeaker). In a first step, each source has been excited successively with white noise to measure directly transfer functions between inputs (signals sent to the shakers and loudspeaker) and responses, to build matrices $\mathbf{H}$ and $\mathbf{\Phi}$. For each excitation configuration with only one active source, the transfer functions have been estimated using a H_1 approach, which is well suited for transfer function measurements with a low noise on inputs. This assumption seems reasonable because input signals are directly measured (without acoustic or vibration transmission) and because they are white (the energy is distributed continuously on the whole frequency range). The transmissibility matrix assessed with $\mathbf{H}$ and $\mathbf{\Phi}$ (Eq. (2)) is considered as the reference transmissibility matrix in the following.

In a second step, the three physical sources were driven by three uncorrelated generators simultaneously to measure the whole response cross-spectral matrix $\mathbf{G_{xyxy}}$. H_1 and H_2 estimators of the transmissibility matrix have been assessed, as well as H_s. For the latter, a scaling has to be applied because different kinds of sensors are used (accelerometers and microphones). The scaling strategy was to normalize all measurement channel by its rms value, thus assuming that the SNR ratio is the same on all channels. One element of the transmissibility matrix is drawn in Fig. 4. All estimators fit the reference transmissibility well on the whole frequency range, even if some errors are visible in low frequency.

The normalized errors, which are computed by means of Eq. (24), are drawn in Fig. 5. It is clear that the estimation error is significantly lower with the H_s estimator on the whole frequency range. In low frequency, H_s and H_2 are similar, and globally better than H_1. In the high frequency range, H_s is similar to H_1, even slightly better, and both are significantly better than H_2.

It can be said globally that the H_s estimator gives better results in this experiment than H_1 and H_2. The applied scaling strategy (normalization of the global levels) was however very basic, and could be improved and optimized to obtain even more satisfying results.

The relative error of H_s is drawn in Fig. 6 (top) in narrow frequency bands in the low frequency range, together with the R indicator defined in Eq. (23). It can be seen that the indicator is in good agreement with the estimation error: it can be said roughly that when the indicator is greater than 10 dB, then the relative estimation error is below 10%. On the other hand, when the indicator drops to almost 0 dB, then the relative error increases and can exceed 100%.

6. Conclusion

Transmissibility matrices are generally estimated using a H_1 like approach. The possibility to use H_2 and H_s estimators for transmissibility matrices is presented. The H_s approach is particularly interesting for the estimation of transmissibility matrices,

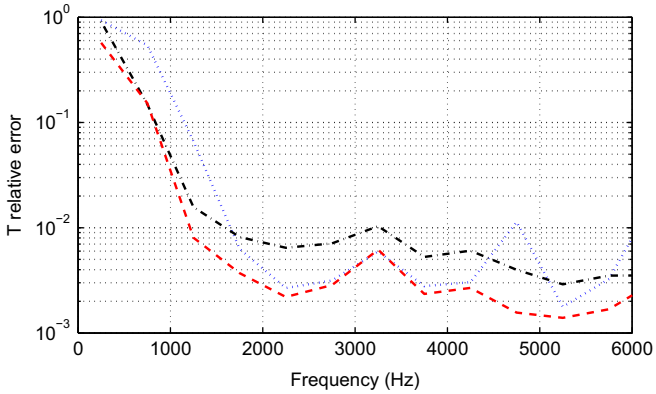

Fig. 5. 500 Hz frequency band integrated relative errors of H_1 (dotted blue), H_2 (dash-dotted black) and H_s (dashed red) estimates. (For interpretation of the references to color in this figure caption, the reader is referred to the web version of this article.)

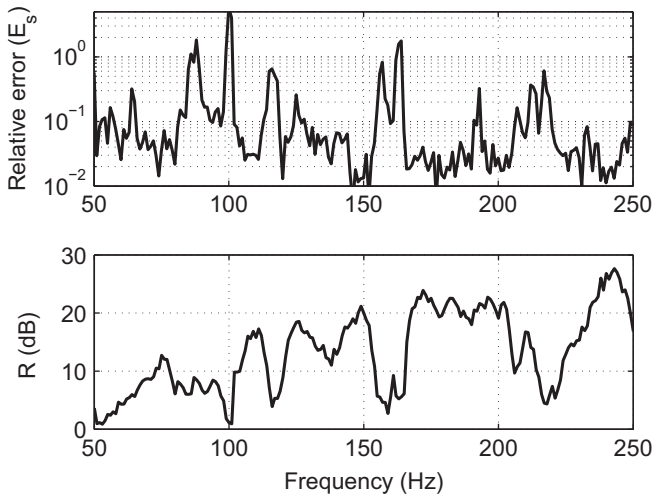

Fig. 6. Relative errors of $H_s[T]$ (top) and corresponding SNR indicator (bottom) in the low frequency range.

because the inputs and outputs of a transmissibility system are both responses, there is thus no reason for the SNR (Signal to Noise Ratio) to be higher on input or output responses. The H_s estimate of the transmissibility matrix is based on the eigenvalue decomposition of the global cross spectral matrix of input and output responses. After a rigorous derivation of the expressions to calculate H_s, it is theoretically shown that H_s tends to H_1 and H_2, depending on the scaling ratios. It is worth noting that the estimator H_2 only exists if the number of output dofs m is equal or larger than the number of indicator dofs n.

Both a numerical simulation and a physical experiment have been conducted to validate the proposed transmissibility estimates. In the numerical simulation a simply supported rectangular plate was considered. In the experiment a plate was excited by means of two shakers and one loudspeaker, constituting two structure borne paths and one airborne path. Both accelerometers and microphones were used, which required some scaling of the data in order to optimize the H_s estimate. For both the numerical simulation and the physical experiment it was found that H_s behaves globally better than H_1 and H_2. In addition, an indicator for the validity of H_s is introduced, which checks that there is a clear separation between the n largest eigenvalues (representing the signal), and the m remaining eigenvalues (representing noise). By approximation, and at least for numerical and experimental illustrations presented in this work, it can be said that for values of the indicator larger than 10 dB, the relative error in the transmissibility estimate is below 10%.

Acknowledgements

This work was performed within the framework of the Labex CeLyA of Université de Lyon, operated by the French National Research Agency (ANR-10-LABX-0060/ ANR-11-IDEX-0007).

Appendix A. Simulation of cross-spectral matrices of uncorrelated finite gaussian signals estimated by the periodogram method

The aim of this Appendix is to explain how cross spectral matrices are randomly generated for measurement simulations. Studied signals are considered to be Gaussian:

$$x[n] = \mathcal{N}(0;\ \overline{x}),$$

where $\overline{x}$ stands for the rms value of the signal. The discrete Fourier Transform of x is given by

$$X_k = \frac{1}{N}\sum_{n=0}^{N-1} x[n] e^{-j2\pi kn/N}$$

with the following expected value and variance:

$$\mathbf{E}(X_k) = 0 \quad \mathbf{V}(X_k) = \overline{x}^2/N$$

with $\mathbf{E}(X_k) = 0$ and $\mathbf{V}(X_k) = \overline{x}^2/N$. X_k follows a complex Gaussian law for $k \neq \{0, N/2\}$, the real and imaginary parts following real centered Gaussian laws of variance $\overline{x}^2/2N$. For $k = \{0, N/2\}$, X_k follows a real centered gaussian law of variance $\overline{x}^2/N$, but this case will not be treated here for the sake of brevity. The double sided instantaneous autospectrum for $k \neq \{0, N/2\}$ is equal to

$$S^i_{xx_k} = 2|X_k|^2 = 2\mathcal{R}(X_k)^2 + 2\mathcal{I}(X_k)^2 = \frac{\overline{x}^2}{N}\chi^2_2$$

with the following expected value and variance:

$$\mathbf{E}\left(S^i_{xx_k}\right) = \frac{2\overline{x}^2}{N} \quad \mathbf{V}\left(S^i_{xx_k}\right) = \frac{4\overline{x}^4}{N^2}$$

The expected value and variance of the double sided instantaneous cross spectrum $S^i_{xy_k} = 2X_k Y_k^*$ of two independent signals x and y are

$$\mathbf{E}\left(S^i_{xy_k}\right) = 0 \quad \mathbf{V}\left(S^i_{xy_k}\right) = \frac{4\overline{x}^2\overline{y}^2}{N^2}$$

When applying the averaged periodogram method, auto and cross spectra are averaged over a number M of time windows:

$$S_{xx_k} = \langle |X_k|^2 \rangle_M \quad S_{xy_k} = \langle X_k Y_k \rangle_M$$

Assuming that M is sufficiently high to apply the central limit theorem, then averaged auto and cross spectra are following Gaussian distributions:

$$S_{xx_k} = \mathcal{N}\left(\frac{2\overline{x}^2}{N};\ \frac{2\overline{x}^2}{N\sqrt{M}}\right) \quad S_{xy_k} = \mathcal{N}\left(0;\ \frac{2\overline{x}\ \overline{y}}{N\sqrt{M}}\right), \quad k \in]0, N/2[$$

It is finally possible to simulate whole cross spectral matrices of uncorrelated signals using a Gaussian random generator, from signals rms values, fixing values for N (number of samples of a time window) and M (number of time windows).

References

[1] S. Chesné, A. Deraemaeker, A. Preumont, On the transmissibility functions and their use for damage localization, in: International Workshop on Structural Health Monitoring (IWSHM 09), Stanford, CA, USA, 2009.
[2] C. Devriendt, P. Guillaume, The use of transmissibility measurements in output-only modal analysis, Mechanical Systems and Signal Processing 21 (7) (2007) 2689–2696.
[3] C. Devriendt, G. De Sitter, P. Guillaume, An operational modal analysis approach based on parametrically identified multivariable transmissibilities, Mechanical Systems and Signal Processing 24 (5) (2010) 1250–1259. Special Issue: Operational Modal Analysis.
[4] P. Gajdatsy, K. Janssens, Wim Desmet, H. Van der Auweraer, Application of the transmissibility concept in transfer path analysis, Mechanical Systems and Signal Processing 24 (7) (2010) 1963–1976. Special Issue: ISMA 2010.
[5] N.B. Roozen, Q. Leclere, C. Sandier, Operational transfer path analysis applied to a small gearbox test set-up, in: Proceedings of Acoustics 2012, Nantes, France, 2012.
[6] A.M.R. Ribeiro, J.M.M. Silva, N.M.M. Maia, On the generalisation of the transmissibility concept, Mechanical Systems and Signal Processing 14 (1) (2000) 29–35.
[7] J.S. Bendat, A.G. Piersol, Engineering Applications of Correlation and Spectral Analysis, Wiley-Interscience, New York, 1980.
[8] A.L. Wicks, H. Vold, The hs frequency response function estimator, in: Proceedings of the 4th International Modal Analysis Conference, Los Angeles, CA, USA, 1986.
[9] P.R. White, W.B. Collis, Analysis of the tls frequency response function estimator, in: Proceedings of the Ninth IEEE workshop on Statistical Signal Processing, Portland OR, USA, 1998.
[10] M.H. Tan, J.K. Hammond, A non-parametric approach for linear system identification using principal component analysis, Mechanical Systems and Signal Processing 21 (4) (2007) 1576–1600.
[11] S.M. Price, R.J. Bernhard, Virtual coherence: a digital signal processing technique for incoherent source identification, in: Proceedings of IMAC 4, Schenectady, NY, USA, 1986.
[12] Q. Leclere, C. Pezerat, B. Laulagnet, L. Polac, Different least squares approaches to identify dynamic forces acting on an engine cylinder block, Acta Acustica 90 (2004) 285–292.
[13] Q. Leclere, C. Pezerat, B. Laulagnet, L. Polac, Indirect measurement of main bearing loads in an operating diesel engine, Journal of Sound and Vibration 286 (2005) 341–361.